Materials Science and Engineering C 37 (2014) 148–155

Contents lists available at ScienceDirect

Materials Science and Engineering C

journal homepage: www.elsevier.com/locate/msec

Development of porous titanium for biomedical applications: A comparison between loose sintering and space-holder techniques

Yadir Torres [a], Sheila Lascano [b], Jorge Bris [c,*], Juan Pavón [d], José A. Rodriguez [a]

[a] Department of Mechanical & Materials Engineering, E.T.S. de Ingenieros, Universidad de Sevilla, Avda. Camino de los Descubrimientos s/n., 41092 Sevilla, Spain
[b] Department of Mechanical Engineering, Universidad Técnica Federico Santa María, Avda. Vicuña Mackenna N° 3939, San Joaquín, Santiago, Chile
[c] Department of Mechanical Engineering, Universidad del Norte, Km. 5 via Pto. Colombia, Barranquilla, Colombia
[d] Group of Advanced Biomaterials and Regenerative Medicine, Bioengineering Program, Universidad de Antioquia, Calle 67 No. 53-108, Medellín, Colombia

ARTICLE INFO

Article history:
Received 24 July 2012
Received in revised form 4 November 2013
Accepted 26 November 2013
Available online 5 December 2013

Keywords:
Porous titanium
Powder metallurgy
Loose-powder sintering
Space holder
Biomedical application

ABSTRACT

One of the most important concerns in long-term prostheses is bone resorption as a result of the stress shielding due to stiffness mismatch between bone and implant. The aim of this study was to obtain porous titanium with stiffness values similar to that exhibited by cortical bone. Porous samples of commercial pure titanium grade-4 were obtained by following both loose-sintering processing and space-holder technique with NaCl between 40 and 70% in volume fraction. Both mechanical properties and porosity morphology were assessed. Young's modulus was measured using uniaxial compression testing, as well as ultrasound methodology. Complete characterization and mechanical testing results allowed us to determine some important findings: (*i*) optimal parameters for both processing routes; (*ii*) better mechanical response was obtained by using space-holder technique; (*iii*) pore geometry of loose sintering samples becomes more regular with increasing sintering temperature; in the case of the space-holder technique that trend was observed for decreasing volume fraction; (*iv*) most reliable Young's modulus measurements were achieved by ultrasound technique.

1. Introduction

Bone degradation related to trauma and disease, as well as its consequent replacement, is considered a public health problem today, which affects one in seven North Americans [1]. This tissue degradation is evident by density reduction above the age of 30 years old, which involves a strength reduction of up to 40% which could be increased by both the cyclic loading and surface wear of joints [2]. These facts can be supported through statistics such as those provided by the *American Dental Association* [3] indicating that 113 million North American adults have lost at least one tooth and 19 million are edentulous. It has also been reported that 10–15% of implants fail in the first 10 years, and 20% of the surgeries are carried out to replace failed implants [4]. Furthermore, the demand for implants is still growing as a result of the rise in life expectancy (13% of the population in the USA are aged 65 years or older; an increase of 8% more has been forecasted for 2050 [5]). Moreover, in younger patients the need for prostheses is also rising, which implies that implants will be subjected to higher levels of mechanical loading for longer periods of time. In this context, further research is needed to develop methodologies that can improve in vivo performance of all implantable devices.

Among all biomaterials employed for bone replacement, it is recognized that titanium and its alloys are those with the best in vivo behavior. Despite this, implant fixation to the bone remains an aspect to be improved through alternatives for reducing the stress-shielding phenomenon, which is a consequence of the mismatch between Young's modulus values (Titanium is 110 GPa and cortical bone around 20–30 GPa); this difference has been identified as one of the major reasons for implant loosening [6–8] and bone resorption. Furthermore, it has been suggested that when bone loss is excessive, it can compromise the long-term clinical performance of the prosthesis [9]. This may also be responsible for implant migration, aseptic loosening, fractures around the prosthesis, and can imply technical problems during revision surgery [9].

Although titanium and its alloy (Ti-6Al-4 V) are the metallic biomaterials with the lowest elastic modulus value (50% lower than Co–Cr), the mismatch with respect to bone stiffness remains a challenging problem that still needs to be addressed. Manufacturing of implants with lower stiffness materials could be a solution for the stress shielding phenomenon [10]. In that sense, development of porous materials is an alternative approach to achieve a stiffness reduction. However, an important issue with the use of porous implants for load bearing applications is the risk of reduction of both mechanical strength and fatigue resistance because the material must be able to withstand the loads without failure. Therefore, to get a desired balance between strength and stiffness is the most important challenge of this approach and has to be accomplished.

There is some ongoing work and developments about biocomposites and porous titanium implants that still do not fulfill the suitable

* Corresponding author at: Departmen of tMechanical Engineering Universidad del Norte Barranquilla - Colombia.
E-mail address: ytorres@us.es (Y. Torres).

0928-4931/$ – see front matter © 2013 Elsevier B.V. All rights reserved.
http://dx.doi.org/10.1016/j.msec.2013.11.036

equilibrium between mechanical and biofunctional properties [11–14]. Several workers have previously shown that it is possible to match the stiffness of cortical bone by using different techniques to produce porous titanium samples [15–25], however, there is a lack of studies about relationships between processing parameters, microstructure and the effect of porosity on the mechanical properties of porous titanium samples.

Porous titanium can be produced by several methods such as loose powder sintering [26,27], slurry foaming [28], reactive sintering [29], hollow sphere sintering [16] and entrapped gas techniques [30]. However, the production of porous materials via the conventional powder metallurgy (PM) route can be cost effective, flexible and lead to the desired design foams [20]. In addition, most of the above-mentioned methods provide limited porosity. Recently, a new powder metallurgy technique using space holder materials (such as carbamide [20,31], NaCl [32,33], K_2CO_3 [34], PMMA [35,36]) has been developed, which has the advantages of great uniformity, adjustable porosity amount, controlled pore shape, and more uniform pore size distribution [37–43].

In this work, loose-sintering and space-holder techniques were used to manufacture porous cpTi samples and the influence of processing on both their microstructural and mechanical properties was investigated. The relationships between morphological features and mechanical properties are also rationalized.

2. Experimental

2.1. Materials

Commercially Pure titanium powder (cp Ti) produced by a hydrogenation/dehydrogenation process was used as the starting powder. The particle size distribution, according to the supplier SE-JONG Materials Co. Ltd., Korea, exhibited particles with irregular morphology and sizes, corresponding to 10%, 50% and 90% passing percentages, of 9.7, 23.3 and 48.4 μm, respectively. The chemical composition is equivalent to commercially pure titanium ASTM F67-00 Grade IV. The space holder used was NaCl (Panreac, purity > 99.5%) due its undemanding decomposition. The concentration of NaCl was within a range of 40–70vol.%, which was similar to that used in previous papers [14,20,44]. The NaCl granules employed as space-holder presented particle sizes corresponding to 10%, 50% and 90% passing percentages, of 183, 384 and 701 μm, respectively. The authors chose a space holder (NaCl) with a large particle size, and cpTi with a fine particle size; there are several reasons for this: (i) A wider NaCl particle distribution (which promotes a higher degree of interconnectivity of the pores), and a high average size of space-holder (>100 μm) would fulfill the requirements to ensure the growth of bone into the implant (ingrowth); (ii) On the other hand, the choice of a titanium powder of irregular shape and small average size would improve the sinterability of the compact (quality of the neck and lower grain size); this will also help to offset the loss of mechanical strength inherent in increased porosity.

2.2. Processing of porous titanium

Two different PM techniques were used: loose-powder sintering and space-holder technique. A sketch illustrating the processing stages for both methods is shown in Fig. 1.

Loose-powder sintering is a method in which the metal powder is poured or vibrated into a mold which is then heated to the sintering temperature in an appropriate atmosphere [27]. Fig. 1a represents the loose-sintering process applied to porous cpTi powder blended for 40 min in a TURBULA T2C mixer. Subsequently, the powder was vibrated into a cylindrical mold of alumina for 2 min. This was a measure of densification of the powder. Finally, the sample was heated to 1000 °C and 1100 °C for 2 h, in a CARBOLYTE STF 15/75/450 ceramic furnace with a horizontal tube under high vacuum ($\sim 5 \times 10^{-5}$ mbar). The above processing conditions were chosen in order to obtain mechanical properties (Young modulus and yield strength) similar to the cortical bone [45].

The space-holder technique is a recently developed PM method that allows porous structures to be obtained with controlled porosity and an enhanced homogeneity. A sketch of the aforementioned process is shown in Fig. 1b. The powder metallurgy technique used to manufacture these samples consisted of a conventional process: 1) mixing of the titanium powder and NaCl particles for 40 min in order to ensure a good homogenization, 2) compaction of the mixture (pressure of 800 MPa, defined according to compressibility curves of materials and the results of a previous work [2,46]), 3) subsequently, the salt was dissolved with distilled water (50–60 °C), in cycles of 240 min (see details in previous work [2,46]), and 5) finally, the sintering temperature was fixed at 1250 ºC for 2 h under high vacuum [2,46].

In both methodologies, the powder mass used to obtain specimens with dimensions suitable for testing compression (height/diameter = 0.8) was overestimated and varied between 2.0 and 2.1 g in order to ensure the desired ratio for compression testing, as well as to avoid the effect of some losses during handling and cutting of the samples. The compaction step was carried out by using an INSTRON 5505 universal machine to apply the pressure needed for the desired porosity, followed by a MALICET ET BLIN U-30 universal machine in order to remove the samples from the matrix. The compaction loading rate was 600 kgf/s, the dwell time was 2 min and the unloading time was 15 s for decreasing loads up to 15 kgf.

2.3. Microstructural and mechanical characterization

The density measurement was carried out by using the Archimedes method with distilled water impregnation, due to its experimental simplicity and reasonable reliability (ASTM C373-88). The total porosity P(Arch) and interconnected porosity (Pi) were calculated from the density measurements by using well known mathematical expressions [47].

For the image analysis, the sectioned parts were prepared by a sequence of conventional metallographic steps (resin mounting, grinding and polishing) followed by a mechano-chemical polishing with magnesium oxide and hydrogen peroxide. Conventional optical microscopy (OM) was also used for the basic observation of the microstructural features of the samples. The porosity evaluation by image analysis was performed by using an optical microscope NIKON EPIPHOT coupled with a JENOPTIK PROGRES C3 camera, and suitable analysis software (IMAGE-PRO PLUS 6.2). The following morphological pore parameters were estimated by this method: the total porosity (P_{IA}), equivalent diameter (D_{eq}) [48] defined as the average diameter measured from the pore centroid, and aspect ratio ($F_f = 4\pi A/(PE)^2$) [48], where A was the pore area and PE was the experimental perimeter of the pore representing a measure of roundness of the pores. Zero values correspond to maximum irregularity and values closer to 1 match with more spherical pores. The mean free path between the pores was defined as the average size of the necks between the pores (λ) [49], and the pore interconnectivity (C_{pore}) defined as the fraction of connected pores of the total reference line length [50].

For mechanical compression testing, the specimen dimensions were fixed according to those recommended (height/diameter = 0.8) in Standard ASTM E9-89A [51]. The yield strength, relative strength (defined as the ratio between the strength of porous material and the solid material) and the Young's Modulus were also obtained. Furthermore, the dynamic Young's modulus measurements using the ultrasound technique were performed with KRAUTKRAMER USM 35 equipment which was used to estimate both longitudinal and transverse propagation velocity of acoustic waves (ASTM E494-10). For each case the PANAMETRICS probe and a suitable ultrasonic couplant fluid was used. Once the acoustic wave velocities were measured, the dynamic Young's modulus was calculated using a known mathematical expression [52].

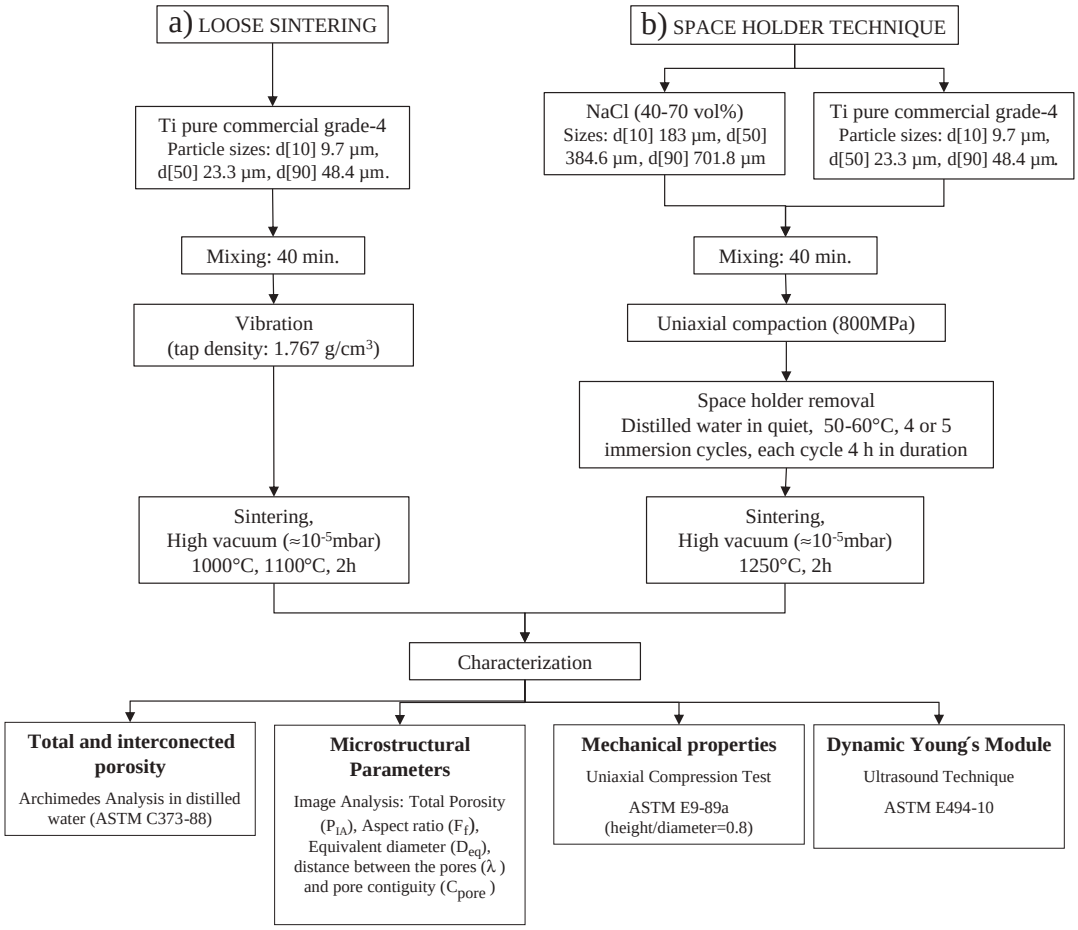

Fig. 1. The processing stages in the powder-metallurgy technique: (a) loose-powder sintering method, and (b) space-holder technique using NaCl.

3. Results and discussion

In order to identify the most important parameters and their working range, the first step of the experiment was the data screening. Variables influencing the space-holder technique are associated with NaCl content, mixing time, compaction pressure, sintering temperature and time, mould features and cooling and dissolution procedures; each one of these factors affects the quality of the obtained porous samples. A large number of samples were tested in this initial screening step, by changing those parameters in a wide range, as is shown in Table 1. In a previous study, the influence of water temperature, agitation and time of dissolution were evaluated [2,46]. As a result, it was found that although many controlling factors affect the process, the output quality was mainly influenced by five parameters: NaCl volume fraction (NaCl vol.%), temperature of water, time of dissolution, compaction pressure and sintering time (t).

In the present study, the influence of NaCl fraction, compact pressure and sintering temperature were further evaluated. The pressures and temperatures were 0 MPa and 800 MPa and 1000 °C, 1100 °C and 1250 °C, respectively. At least three compacts were manufactured for each combination, and Table 2 summarizes the conditions evaluated.

Table 1
Analyzed parameters for the screening.

Factors	Tested range
NaCl fraction (%)	40–70
Mixing time (min)	1–60
Temperature of water (°C)	20–26 and 50–60
water condition	Steady and agitated
Time of dissolution (min)	30, 120, 240
Pressure (MPa)	0, 13.8, 38.5 and 200–800
Temperature (°C)	1000–1300

3.1. Microstructural characterization

According to features observed in Fig. 2, the higher porosity achieved with space-holder technique is the first finding that can be highlighted from comparing the evaluated processing routes.

In loose-powder sintering, the higher porosity was associated with the lowest sintering temperature of 1000 °C, as observed in Fig. 2 (a). For the highest sintering temperature the porosity was reduced and the pores became more isolated. The influence of sintering temperature on pore morphology is shown in Fig. 3a and b. Moreover, quantitative results for 1000 °C and 1100 °C obtained by the Archimedes method and Image Analysis support the qualitative aspects assessed previously (Fig. 3(c) and (d)). In that sense, several parameters were evaluated: equivalent diameter (D_{eq}), total porosity obtained by Archimedes ($P_{Arch.}$) and image analysis (P_{IA}), the aspect ratio (F_f), distance between the pores (λ), and the pore interconnectivity (C_{pore}). The statistical distribution depicted in Figs. 2 and 3, where the columns are of equivalent diameter (D_{eq}), shows a quantitative representation of the pore size. The height of the bell decreases with increasing temperature; the

Table 2
Experimental factors and levels.

Factors	Level 1	Level 2	Level 4	Level 5	Level 6	Level 7
NaCl fraction (vol. %)	0		40	50	60	70
Pressure (MPa)	Vibrated		800			
Sintering temperature (°C)	1000	1100	1250			

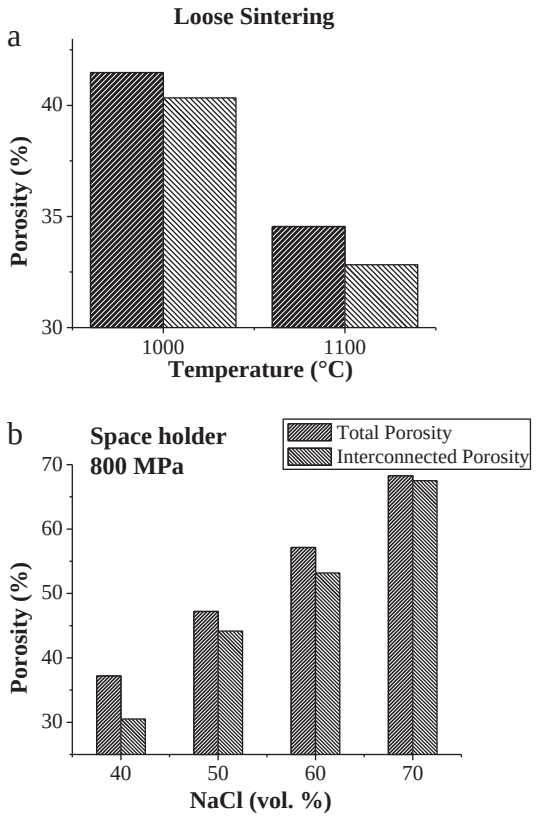

Fig. 2. Effect of the processing parameters on the total and interconnected porosity: (a) influence of the temperature for loose-sintering process; (b) influence of NaCl content in space-holder technique at 1250 °C.

pores also appear smaller and even more homogeneous. On the other hand, the highest frequency value of D_{eq} was 10 μm. However, the aspect ratio, F_f, keeps constant for highest sintering temperature; i.e. pores exhibit basically the same inner roughness and spherical contours. In addition, the pore interconnectivity (C_{pore}) was smaller when the temperature was increased, which also indicates that pores are more isolated (distance between the pores, λ, is larger). Higher values of C_{pore} were found at 1000 °C, implying that samples processed at sintering temperatures of 1000 °C exhibited more spherical and interconnected pores with an equivalent diameter of 10 μm. Despite all these porosity features being unexpected, they can certainly be explained as follows: the porosity and the pore size are usually high in those samples obtained by loose-powder sintering. For the higher sintering temperature, the lower porosity is obtained (41.5% vs. 34.6%, for 1000 ºC and 1100 ºC, respectively). However, the pore size has an opposite trend (16 μm vs. 18 μm, for 1000 ºC and 1100 ºC, respectively); as a consequence of this, pores are larger and even more irregular (less spherical contours).

From general inspection of processed samples, it was observed that porous titanium with porosities in the range of 40–70 vol.% was successfully made by using NaCl as space holder. The effect of NaCl content is shown in Fig. 4. Two types of pores have been observed in these same samples: interconnected macropores mostly left by the space holder, and isolated micropores obtained during the partial sintering of the titanium powders on the pore walls. With respect to those isolated pores, Fig. 4 also illustrates that they are also of two kinds, from morphological point of view: some of them have a rounded shape, whilst some others are more of cubic shape; these latter are the consequence of the initial shape of the space holder powder. This observation implies that any approach made here about assumptions of mostly rounded pores will obviously have some limitations due to actual existence of some cube shape pores.

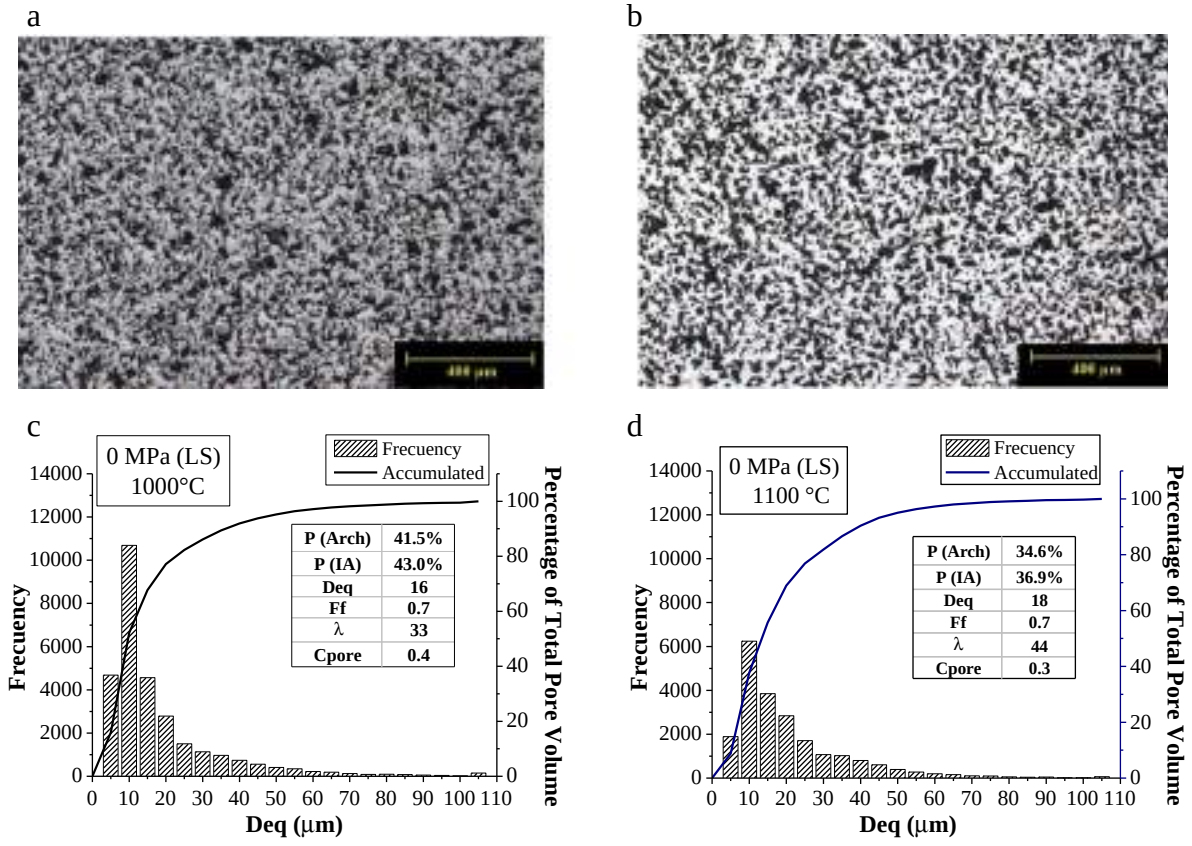

Fig. 3. Typical porosity obtained by loose powder sintering method at different temperatures: (a) 1000 °C, (b) 1100 °C, and effect of the temperature on the morphological characteristics of the pores, (c) 1000 °C and (d) 1100 °C. The major porosity was reached at 1000 °C (41.5%). The pores were more interconnected at the lower sinter temperature.

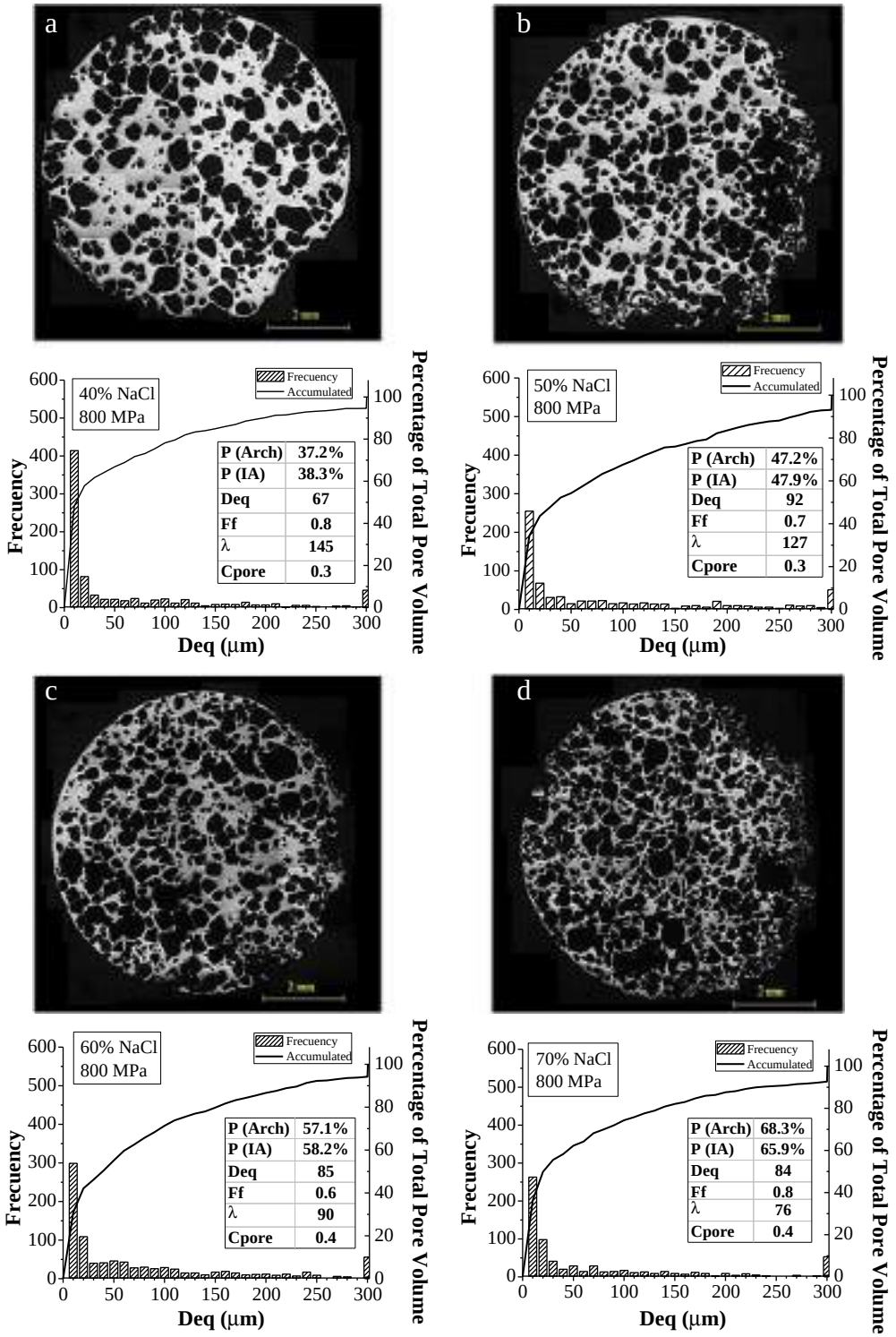

Fig. 4. Typical porosity obtained by space-holder technique, using different space-holder percentage of NaCl vol. % and the effect of the space-holder content on the morphological characteristics of the pores: a) 40%, b) 50%, c) 60%, and d) 70%. The highest porosity was reached with 70% NaCl (68.3%).

Regarding the porosity parameters for the lowest values of NaCl content, the samples appeared with smaller, and mostly isolated and more spherical pores, with some cube shape pores as it was mentioned above: *i)*. Around 50% of the powder particles for 40 vol.% NaCl vs. 30% of the powder particles for 70 vol.% NaCl, had a particle size <10 μm, *ii)* Parameters like $\lambda = 144.7$ μm for 40 vol.% NaCl vs. 76.1 μm for 70 vol.% NaCl, and *iii*) Some other values such as $F_f = 0.77$ for 40 vol.% NaCl vs. $F_f = 0.60$ for 60 vol.% NaCl, were produced. These characteristics were confirmed by image analysis results. The statistical distribution of the pores is also shown in Fig. 4. A large amount of pores with a diameter up to 100 μm, available to possible bone ingrowth, were found. At the same time, the porosity obtained after sintering was proportional to the initial NaCl content (e.g. 68.3% vs. 70 vol.% NaCl initially).

The above results show that the space-holder technique allows higher porosity values by comparison with Fig. 2. The maximum porosity and diameter of the pores that were achieved through the loose-sintering technique were 41.5% and 16 μm for 1000 °C, respectively, compared to 68.3% and 84 μm respectively, obtained with the space-

holder technique. More interconnected porosity was achieved by the space-holder technique (see Figs. 3 and 4). The results of the image analysis for specimens obtained by both loose-powder sintering and space-holder technique are summarized in Table 3.

3.2. Mechanical characterization

Fig. 5 shows the curves of compression stress vs. strain obtained from cpTi porous samples. The first feature from this figure is that curve behavior is correlated with the total porosity of the samples. As expected, both compression strength and Young's modulus decrease as the porosity increases. The compression strength is higher as the temperature increases in loose-powder sintering; this trend is related to the increasing Ti remaining in the matrix (λ), as well as to softer pore contours (greater F_f), and also with the better quality of the sintering necks; these three factor are the predominant ones, despite the slight increase in the pore size which is inherent to enhanced coalescence with the sintering temperature. This result has been compared with previous studies reported by the authors [45,53], in which they evaluated the porosity limits (associated Young's modulus) that can be achieved by conventional powder metallurgy routes. On the other hand, it can also be noticed from Fig. 5 that the yield strength of space-holder samples also increases when both the NaCl content and pore size decrease (least amount of NaCl particles interconnected). This technique allows higher porosities to be obtained and better mechanical performances to be achieved due to a higher quality of sintering necks, which is a consequence of a higher sintering temperature (the porosity was preserved due to the space-holder material used). Interestingly, Fig. 5 also highlights the lower mechanical strength exhibited from the space holder sample with lowest porosity (37.2%), compared with the loose sintered sample with the highest porosity (41.5%). This apparently unexpected difference can be explained in terms of porosity factors that influence mechanical strength in these porous solids: despite the total and interconnected porosities of that space holder sample being smaller (see Fig. 2), values of D_{eq} and λ are higher, and C_{pore} is also smaller (see Figs. 3 and 4); therefore, it can be assumed that these three parameters are mechanically dominant and, therefore, they can explain the different responses between these samples.

None of the conditions evaluated in this research matches with cortical bone requirements (mechanical strength), except the compacts made with a 40 vol.% of NaCl. Also, in these samples pore sizes of between 50 and 100 μm (see Fig. 4) and some roughness characteristics within the pores were observed [46]. These latter findings suggest some potential bone ingrowth capability of the porous samples (with the consequent increase in mechanical strength), which can also improve Ti implant osteointegration.

Some authors have developed models in order to address explanations about relationships between porosity and mechanical strength in sintered materials. One of those approaches [54] is based on the geometric relationship between the porosity and the effective area, by considering pores with a perfectly spherical geometry. On the other hand, Hyun et al. [55] validated their model with results obtained from porous

Table 3
Summary of the pore's structural features.

Parameters	Temperature (°C)		NaCl vol. %			
	1000	1100	40	50	60	70
Total porosity by Archimedes method—P (Arch.) (%)	41.5	34.6	37.2	47.2	57.1	68.3
Total porosity by image analysis—P (IA) (%)	43.0	36.9	38.3	47.9	58.2	65.9
Aspect ratio—Ff	0.7	0.7	0.8	0.7	0.6	0.8
Equivalent Diameter—D_{eq} (μm)	16	18	67	92	85	84
Distance between pores—λ (μm)	33	44	145	127	90	76
Pore interconnectivity—C_{pore}	0.4	0.3	0.3	0.3	0.4	0.4

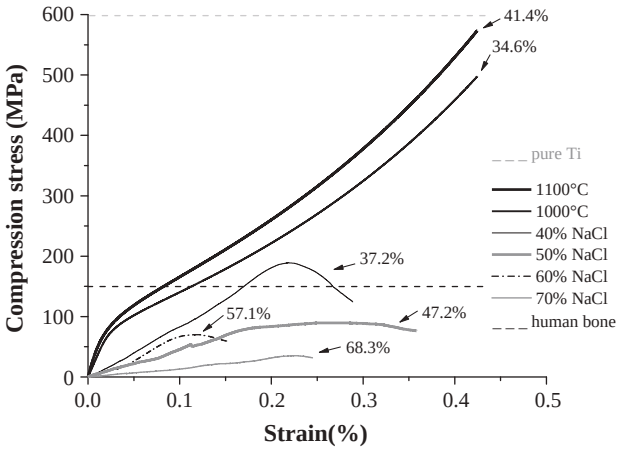

Fig. 5. Compression stress–strain curves of samples having various amounts of porosity and obtained by the loose-sintering and space-holder technique.

copper by assuming cylindrical-shaped pores with a perpendicular orientation with respect to the direction of applied load. On the other hand, the "simple brick" model [56] assumes cubic pores and determines the relative strength according to the probability of finding a solid fraction of volume. Finally, the model of Griffiths et al. [57] considers porosity as a distribution of spheres and oval ellipsoids including a λ parameter that represents porous shape factor. The relationship between the relative strength and the density is represented in Fig. 6, where a lack of correlation can be observed. None of them is a real model of the behavior obtained in this study. A new model with a better correlation is currently being developed by the authors and will be published soon. However, some expected results were observed: the strength decay produced by a porosity increment is even more pronounced; this relationship actually confirms that pores act like notches which produce stress concentration ("notch strengthening"), besides reducing strength effective area. Within this context, it is expected that some change from a close to open porosity regime will generate a triaxial effect that can partially compensate for strength loss associated with any increasing of porous fraction. Therefore, under interconnected porosity conditions, yield strength will not be drastically reduced due to porosity increments, which is the case when isolated porosity is increased. Fig. 6 illustrates a slope change similar to that reported in other PM materials, for a density value around 2.2–2.3 g/cm^3 (45% of interconnected porosity).

Estimations of Young's Modulus by both conventional compression testing and the dynamic method in terms of porosity samples are presented in Fig. 7. These results were compared with conventional PM experimental values [24,45,53], as well as with the models proposed by

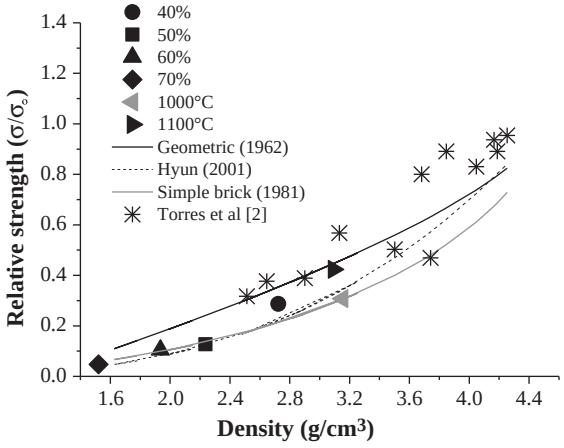

Fig. 6. Density vs. relative strength.

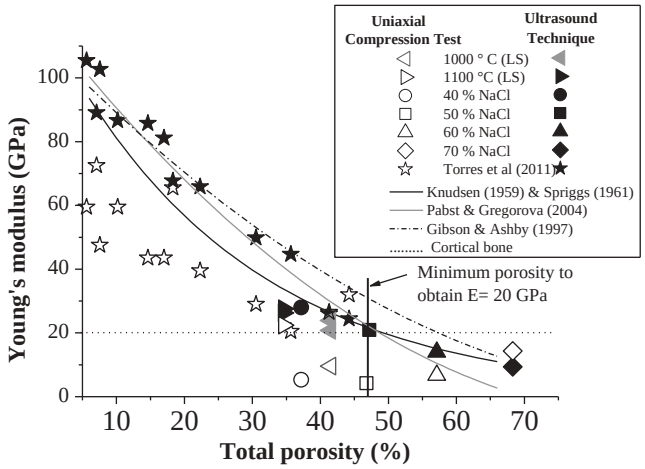

Fig. 7. Young's modulus vs. total porosity. Reference line: 20 GPa (Young's modulus of human cortical bone). Influence of the porosity in the dynamic Young's modulus compared with other authors.

Knudsen [58] and Spriggs [59], Pabst and Gregorová [60], Gibson and Ashby [61] and Nielsen [62] (see Fig. 7), and with the experimental Young's modulus value of cortical bone (20 GPa). Afterwards, in order to check the similarities between the experimental modulus and Nielsen approach, the fixing was analyzed between the points represented in Fig. 8 with a 45° straight line. From Fig. 8 it is clear that Young's modulus measurements from ultrasound technique present the best fix with respect to calculations from the Nielsen model (Eq. (1)). On the other hand, measurements obtained from compression tests show an important deviation for highest Young's modulus values. Therefore, the ultrasonic testing technique is a more reliable way to measure the Young's modulus.

$$E_{Nielsen} = E_{Ti}\left[\frac{\left(1-\frac{P}{100}\right)^2}{1+\left(\frac{1}{F_f}-1\right)\times\frac{P}{100}}\right] \quad (1)$$

The evaluation of Young's modulus in porous materials is controversial. Young's modulus measurements from uniaxial compression tests are significantly lower than dynamic measurements. Greiner et al. [63] associated this discrepancy with super-elastic deformation within the linear–elastic range of NiTi materials; stiffness measured by ultrasonic technique decreases with increasing porosity, in agreement with elastic

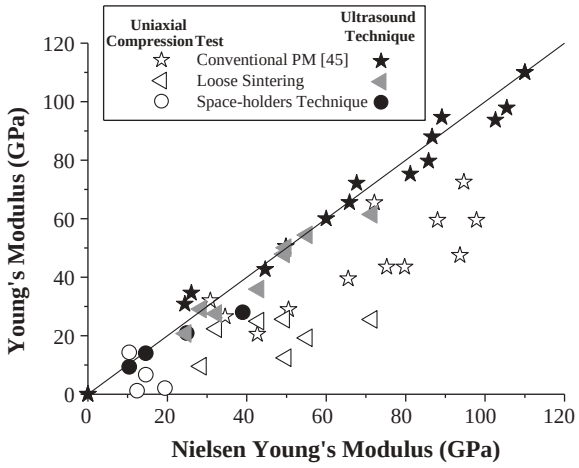

Fig. 8. Comparison between the Young's modulus obtained by both compression and ultrasound tests with the Nielsen approach.

Eshelby-based theory for closed, spherical porosity [64,65]. Torres et al. [45] reported a similar trend for C. P. Ti obtained by a conventional powder-metallurgy process, as well as in recent work developed with space-holder (NH_4HCO_3) [66]. These authors related this difference to a stiffness testing machine effect in which the mechanical system and sample were considered as two springs in series. Moreover, it must be remembered that the Ti matrix is different at each cross-section of the cylindrical sample during a compression test; the material collapse starts at the section with the lowest Ti content. However, in the ultrasonic technique, the Young's modulus is estimated as a function of the wave velocity, which goes through all of the sections of the sample. Therefore, a change in one of four parameters (time of transfer, attenuation, reflection and frequency) associated with the high frequency waves transition from side to side of the material, could be linked with variations of physical properties such as Young's modulus, density or homogeneity in the microstructure.

Fig. 7 shows a wide spectrum of possible porosities and Young's moduli corresponding to a wide range of processing conditions. From this graph, it is evident that the higher porosity, the lower is the Young's modulus obtained. However, it is more interesting to note the confirmation of the inverse relationship between Young's modulus and NaCl content and the direct trend with sintering temperature. Regarding the Young's modulus sought for cortical bone replacement (~20 GPa), it can be noted that the corresponding porosity was ~45% and the suitable processing conditions were 50 vol.% of NaCl (space-holder technique) and 1000 ºC (loose-powder sintering processing). The use of the space-holder technique allows the possibility of obtaining the mechanical requirements of the cortical bone: yield strength (>150 MPa), an appropriate Young's modulus (solving the stress shielding phenomena) and an equivalent diameter D_{eq} superior to 50–100 μm (to promote the bone in-growth). Although in some samples a Young's modulus similar to the bone was reached, their mechanical strength was poor (Fig. 6). However, it is expected that even in these cases the mechanical strength of integrated implant will be suitable due to the bone in-growth during the patient recovery time; this intimate contact with the bone will reduce any stress concentration effect associated with surface porosity.

4. Conclusions

According to the results achieved in assessing the influence of loose-powder sintering and space-holder technique conditions in both microstructural and mechanical properties of porous Ti for bone replacement, the following findings can be drawn:

- Porous samples of commercially pure titanium (grade 4) were obtained using loose-powder sintering technique. The better stiffness results (20 GPa to 25 GPa against 20–30 GPa of cortical bone) were achieved for the lowest values of sintering temperature (1000 °C), with porosity around 41.5%.
- The most suitable stiffness value of the porous cpTi samples obtained by space-holder technique was achieved with a porosity of about 47%, with interconnected pores and also with an appropriate size and even with a better aspect ratio. These results were better than those obtained through loose-powder sintering. Therefore, the mechanical properties were improved because of the enhanced quality of the sintering necks.
- Regarding the pore geometry obtained in this work, it becomes more regular with decreasing sintering temperature for the case of loose-powder sintering. With respect to space-holder technique, that effect was observed for a decreasing volume fraction of space-holder component.
- Ultrasound technique used for dynamic Young modulus estimation of porous titanium samples has shown to be a suitable tool for the study of this kind of material. This was reasonably verified by comparison of the measurements obtained by this technique with the values

calculated from the Nielsen theoretical model, which includes experimentally determined porosity parameters.

Acknowledgments

This work was supported by the Ministry of Science and Innovation in Spain (MAT2010-20855). The authors wish to thank the laboratory technicians J. Pinto, J. M. Recio and I. Nieto for carrying out the microstructure characterization and mechanical testing. The funding given by "*El Patrimonio Autónomo Fondo Nacional de Financiamiento para la Ciencia, la Tecnología y la Innovación Francisco José de Caldas—Contrato RC-No. 275-2011*" is recognized.

References

[1] R.D. Crowninshield, A.G. Rosenberg, S.M. Sporer, Clin. Orthop. Relat. Res. 443 (2006) 266–272.
[2] Y. Torres, J.J. Pavón, G.B. Hernández, I. Nieto, S. Lascano, J.A. Rodríguez, in: V. Amigó (Ed.), III Congreso Nacional de Pulvimetalurgia, Universitat Politècnica de València, Valencia, Spain, 2010, pp. 455–468.
[3] J.B. Brunski, Metals, in: P.D. Ratner, et al., (Eds.), Biomaterials Science: An Introduction to Materials in Medicine, Elsevier Academic Press, California, 2004, p. 37.
[4] R.O. Ritchie, ASM Intl. Materials and Processes for Medical Devices Conference, St. Paul, Minnesota, 2004.
[5] C.E. Misch, Implant. Dent. 8 (1999) 90.
[6] D.M. Robertson, L. Pierre, R. Chahal, J. Biomed. Mater. Res. 10 (1976) 335–344.
[7] H.U. Cameron, I. Macnab, R.M. Pilliar, Int. J. Artif. Organs 1 (1978) 104–109.
[8] W.C. Head, D.J. Bauk, R.H. Emerson, Clin. Orthop. Relat. Res. 311 (1995) 85–90.
[9] H. Kroger, P. Venesmaa, J. Jurvelin, H. Miettinen, O. Suomalainen, E. Alhava, Clin. Orthop. Relat. Res. 352 (1998) 66–74.
[10] T. Otani, L. Whiteside, Orthop. Clin. North Am. 23 (1992) 335–346.
[11] D.A. Gerard, D.A. Koss, Int. J. Fatigue 13 (1991) 345–352.
[12] T. Imwinkelried, J. Biomed. Mater. Res. A 81A (2007) 964–970.
[13] S. Yue, R. Pilliar, G. Weatherly, J. Biomed. Mater. Res. 18 (1984) 1043–1058.
[14] I.H. Oh, N. Nomura, N. Masahashi, H.S., Scr. Mater. 49 (2003) 1197–1202.
[15] G.E. Ryan, A.S. Pandit, D.P. Apatsidis, Biomaterials 27 (2006) 2651–2670.
[16] D. Dunand, Adv. Eng. Mater. 6 (2004) 369–373.
[17] K. Asaoka, N. Kuwayama, O. Okuno, I. Miura, J. Biomed. Mater. Res. 19 (1985) 699–713.
[18] E. Spoerke, N. Murray, H. Li, L. Brinson, D. Dunand, S. Stupp, J. Biomed. Mater. Res. A 84 (2008) 402–412.
[19] M.M. Dewidar, J.K. Lim, J. Alloy Compd. 454 (2008) 442–446.
[20] N. Wenjuan, B. Chenguang, Q. GuiBao, W. Qiang, Mater. Sci. Eng. A 506 (2009) 148–151.
[21] Y.B. An, N.H. Oh, Y.W. Chun, D.K. Kim, J.S. Park, J.-J. Kwon, K.O. Choi, T.G. Eom, T.H. Byun, J.Y. Kim, P.J. Rucroft, K.J. Kim, W.H. Lee, Mater. Lett. 59 (2005) 2178–2182.
[22] O. R., R. Licheri, A.M. Locci, A. Cincotti, C. G., Mater. Sci. Eng. R. Rep. 63 (2009) 127–287.
[23] T. Traini, C. Mangano, R. Sammons, F. Mangano, A. Macchi, A. Piattelli, Dent. Mater. 24 (2008) 1525–1533.
[24] B.V. Krishna, B. Bose, A. Bandyopadhyay, Acta Biomater. 3 (2007) 997–1006.
[25] G.E. Ryan, A.S. Pandit, D.P. Apatsidis, Biomaterials 29 (2008) 3625–3635.
[26] R.M. German, Powder metallurgy of iron and steel, John Wiley & Sons, USA, 1998.
[27] G.S. Upadhyaya, Powder metallurgy technology, Cambridge Int Science Publishing, England, UK, 2002.
[28] J.P. Li, S.H. Li, K. de Groot, P. Layrolle, Key Eng. Mater. 218 (2002) 51–54.
[29] M. Barrabés, P. Sevilla, J.A. Planell, F.J. Gil, Mater. Sci. Eng. C 28 (2008) 23–27.
[30] N.G.D. Murray, D.C. Dunand, Acta Mater. 52 (2004) 2269–2291.
[31] H. Bafti, A. Habibolahzadeh, Mater. Des. 31 (2010) 4122–4129.
[32] R. Surace, L.A.C. De Filippis, A.D. Ludovico, G. Boghetich, Mater. Des. 30 (2009) 1878–1885.
[33] Y. Bing, D. Dunand, Mater. Sci. Eng. A 528 (2010) 691–697.
[34] Y.Y. Zhao, T. Fung, L.P. Zhang, F.L. Zhang, Scr. Mater. 52 (2005) 295–298.
[35] A. Manonukul, N. Muenya, F. Léaux, S. Amaranan, J. Mater. Process. Technol. 210 (2010) 529–535.
[36] T. Fengqiu, H. Fudouzi, T. Uchikoshi, Y. Sakka, J. Eur. Ceram. Soc. 24 (2004) 341–344.
[37] A. Laptev, M. Bram, D. Buchkremer, D. Stover, Powder Metall. 48 (2005) 358.
[38] G. Kotan, A. Bor, Turk. J. Eng. Environ. Sci. 31 (2007) 149–156.
[39] C.E. Wen, M. Mabuchi, Y. Yamada, K. Shimojima, Y. Chino, T. Asahina, Scr. Mater. 45 (2001) 1147–1153.
[40] Z. Esen, S. Bor, Scr. Mater. 56 (2007) 341–344.
[41] C.E. Wen, Y. Yamada, K. Shimojima, Y. Chino, T. Asahina, M. Mabuchi, J. Mater. Sci. Mater. Med. 13 (2002) 397–401.
[42] M. Bram, C. Stiller, H.P. Buchkremer, D. Stover, H. Bauer, Adv. Eng. Mater. 2 (2000) 196–199.
[43] M.F. Ashby, A.G. Evans, N.A. Fleck, L.J. Gibson, L.W. Hutchinson, H.G. Wadley, Metal foams: a design guide, Butterworth-Heinemann, Elsevier, Oxford, UK, 2000.
[44] Y.J. Chen, B. Feng, Y.P. Zhu, J. Weng, J.X. Wang, X. Lu, Mater. Lett. 63 (2009) 2659–2661.
[45] Y. Torres, J.J. Pavón, I. Nieto, J.A. Rodríguez, Metall. Mater. Trans. B 42 (2011) 891–900.
[46] Y. Torres, J.J. Pavón, J.A. Rodríguez, J. Mater. Proc. Technol. 212 (2012) 1061–1069.
[47] ASTM, C373-88, Standard test method for water absorption bulk density, apparent porosity, and apparent specific gravity of fired whiteware products, 1999.
[48] R.W. Cahn, Adv. Mater. 2 (1990) 111–112.
[49] B. Roebuck, E.A. Almond, Int. Mater. Rev. 33 (1988) 90–112.
[50] Y. Torres, Tesis doctoral, Barcelona, 2002, pp. 21–24.
[51] ASTM, E9-89a, Standard test methods of compression testing of metallic materials at room temperature, 2000.
[52] M. Kikuchi, M. Takahashi, O. Okuno, Dent. Mater. 22 (2006) 641–646.
[53] Y. Torres, J.J. Pavón, I. Nieto, S. Lascano, J.A. Rodríguez, in: V. Amigó (Ed.), III Congreso Nacional de Pulvimetalurgia, Universitat Politècnica de València, Valencia, Spain, 2010, pp. 229–240.
[54] M. Eudier, Powder Metall. 5 (1962) 278–290.
[55] S. Hyun, K. Murakami, H. Nakajima, Mater. Sci. Eng. A 299 (2001) 241–248.
[56] N. Fleck, R. Smith, Powder Metall. 3 (1981) 121–125.
[57] T.J. Griffiths, R. Davies, M.B. Bassett, Powder Metall. 22 (1979) 119–123.
[58] F.P. Knudsen, J. Am. Ceram. Soc. 42 (1959) 373–397.
[59] R.M. Spriggs, J. Am. Ceram. Soc. 44 (1961) 628–629.
[60] W. Pabst, E. Gregorová, J. Mater. Sci. 39 (2004) 3501.
[61] L.J. Gibson, M.F. Ashby, Cellular solids: structure and properties, Cambridge University Press, New York, NY, 1997.
[62] L.F. Nielsen, J. Am. Ceram. Soc. 67 (1984) 93–98.
[63] C. Greiner, S.M. Oppenheimer, D.C. Dunand, Acta Biomater. 1 (2005) 705–716.
[64] J.D. Eshelby, Proc. R. Soc. Lond. A 3 (1957) 376–396(396).
[65] Y.Y. Zhao, M. Taya, J. Appl. Mech. 74 (2007) 291–297.
[66] Y. Torres, J.A. Rodríguez, S. Arias, M. Echeverry, S. Robledo, V. Amigó, J.J. Pavón, J. Mater. Sci. 47 (2012) 6565–6576.